Article:
Tostevin, R and Mills, BJW orcid.org/0000-0002-9141-0931 (2020) Reconciling proxy records and models of Earth's oxygenation during the Neoproterozoic and Palaeozoic. Interface Focus, 10 (4). 20190137. ISSN 2042-8901

https://doi.org/10.1098/rsfs.2019.0137

Reconciling proxy records and models of Earth's oxygenation during the Neoproterozoic and Palaeozoic

Rosalie Tostevin[1] and Benjamin J. W. Mills[2]

[1]Department of Geological Sciences, University of Cape Town, Rondebosch, Cape Town, South Africa.

[2]School of Earth and Environment, University of Leeds, Leeds, LS29JT, UK

Abstract

A hypothesised rise in oxygen levels in the Neoproterozoic, dubbed the Neoproterozoic oxygenation event (NOE), has been repeatedly linked to the origin and rise of animal life. However, a new body of work has emerged over the past decade that questions this narrative. We explore available proxy records of atmospheric and marine oxygenation, and considering the unique systematics of each geochemical system, attempt to reconcile the data. We also present new results from a comprehensive COPSE biogeochemical model that combines several recent additions, to create a continuous model record from 850–250 Ma. We conclude that oxygen levels were intermediate across the Ediacaran and early Palaeozoic, and highly dynamic. Stable, modern-like conditions were not reached until the Late Palaeozoic. We therefore propose that the terms Neoproterozoic Oxygenation Window (NOW) and Palaeozoic Oxygenation Event (POE) are more appropriate descriptors of the rise of oxygen in Earth's atmosphere and oceans.

1. Introduction

Since the Great Oxidation Event, 2.5 – 2.3 billion years ago (Ga), oxygen has been a persistent feature of Earth's atmosphere[1], but has remained at low levels throughout the Palaeoproterozoic and Mesoproterozoic eras (2.5 – 1.0 Ga). A hypothesised rise towards modern oxygen levels in the Neoproterozoic (1.0 – 0.54 Ga) was dubbed the "Neoproterozoic Oxygenation Event" (NOE)[2]. Evidence for the NOE included broad increases in the average molybdenum and vanadium concentrations in black shales[3]; an increase in the isotope fractionation between sulfate and pyrite ($\Delta^{34}S_{SO4\text{-}pyr}$)[4]; and Fe speciation evidence for local deep water oxygenation[5].

Geochemical data collected over the last decade has disrupted this narrative. Despite an increase in the breadth and depth of proxy data now available, we appear to be further from a consensus on the timing and dynamics of oxygenation. Some proxies support a single, unidirectional step change in oxygen levels, although estimates of the timing span almost 600 Myrs[6–15]. Other proxy data support a more dynamic system, with large oscillations in oxygen availability[16–18].

How can we reconcile these different proxy records? One possibility is that some of the geochemical data do not record ancient redox conditions, because they have been overprinted by diagenesis and metamorphism. While some published data may be need to be revisited, other geochemical signals are reproducible in samples from different basins (e.g., Uranium isotopes[18,19], or redox sensitive trace elements[7,17,20,21]). In addition, geochemical redox analysis can be paired with petrography or other geochemical data to screen for potential alteration. Another possibility is that we are misinterpreting primary geochemical signals. Because today's oceans are largely well-oxygenated, proxy systems are

calibrated in isolated basins and lakes, and these environments may not provide a reasonable analogue for a globally anoxic deep ocean. Alternatively, each proxy may be capturing different parts of a complex transition, depending on the proxy systematics, marine residence time, reduction potential, and sampling density. Here, we critically evaluate current proxy evidence for Neoproterozoic–Palaeozoic oxygenation, attempt to reconcile the various records, and compare them to the latest biogeochemical modelling results.

2. Evaluation of current geochemical evidence

2.1 Local Marine Geochemical Proxies

Local marine redox proxies record progressive changes within a single basin[5,22], but if those changes are driven by local hydrodynamics or changes in productivity, they may not reflect global changes in oxygen availability. When sufficient local proxy data are collected from multiple basins, the compiled data may record a statistically significant change in the average oxidation state of the ocean. However, these proxy records are necessarily biased towards shelf and slope environments, as Proterozoic sediments from the abyssal plain are rarely preserved. Proxies preserved in carbonates, such as I/Ca and Ce anomalies, are further biased towards warm, shallow shelf environments at low latitudes.

Iron speciation:

The ratio of highly reactive to total iron preserved in carbonates and shales is indicative of the redox chemistry in the water column directly above the accumulating sediments[23]. Robust calibrations of the proxy in modern sediments allows the differentiation of oxic (Fe_{HR}/Fe_T <0.22) and anoxic water masses (Fe_{HR}/Fe_T >0.38), although ambiguous ratios may

71 be generated under high sedimentation or mixing rates (Fe_{HR}/Fe_T 0.22–0.38). For anoxic
72 water masses, the proportion of pyrite in the highly reactive iron phase can distinguish
73 between Fe-bearing (ferruginous) and sulfidic (euxinic) anoxia (Table 1). Therefore, "oxic"
74 conditions identified by iron speciation could potentially incorporate suboxic and well-
75 oxygenated conditions. Systematic diagenetic biases could be introduced to the iron
76 speciation record through transformation of unsulfidised highly reactive iron minerals to
77 less reactive sheet silicates, producing a false oxic signal.
78
79 A transition towards oxic Fe speciation signals ~580 Ma, recorded in shales deposited on a
80 continental slope, was thought to pinpoint permanent oxygenation of the deep ocean[5].
81 However, as more data have been collected, an increasingly complex picture of spatial and
82 temporal heterogeneity has emerged. For example, data from basins of the same age in the
83 Canadian cordillera show no such oxygenation[21,24], and younger basins record anoxic waters
84 impinging onto the shelf[25]. A recent statistical analysis of 4,700 Fe speciation measurements
85 from deep water settings across a range of ages and locations has revealed no significant
86 long term (i.e., 100 Myr) trend towards more oxic conditions across the Neoproterozoic and
87 early Palaeozoic (Figure 1 and 2)[14]. This study has good spatial and temporal coverage from
88 ~2.1 Ga to 440 Ma, although Silurian–Devonian data come from just two studies and may be
89 subject to sampling biases (Figure 2)[7,26].
90
91 **Table 1**: *Summary of proxy systematics*

	Proxy	**Responds to**	**Redox sensitivity**	**Archives**	**Systematic bias?**
Local/ Regio	Iron speciation	Integrated regional water column redox conditions	Ferruginous anoxia and euxinia	Shales, carbonate	Variable

		above accumulating sediments			
	I/Ca ratios	Upper ocean oxygen gradients	Hypoxic (<70 μM O_2) to suboxic (between manganous and nitrogenous)	Carbonates	False anoxic
	Ce anomalies	Local–regional water column redox at site of carbonate precipitation	Suboxic (manganous)	Carbonates, phosphorites, iron formation	False anoxic
	$\sum Fe^{3+}/Fe$	Regional deep water oxygen concentrations	Progressive with increasing $O_2(aq)$	Basalts	False anoxic
	Marine red beds	Regional deep ocean oxygen concentrations following periods of anoxia	Ferruginous anoxia	Marine red beds	
Global marine	$\delta^{238}U$	Area of global seafloor bathed in anoxic waters	Anoxia	Carbonates, shales	False oxic
	$\delta^{98}Mo$	Area of global seafloor bathed in anoxic waters	Euxinia	Shales	False anoxic
	RSE enrichments	Area of global seafloor bathed in anoxic waters	Euxinia (Mo); ferruginous anoxia (Cr, Re, U, V)	Euxinic shales	False anoxic
	$\delta^{82}Se$	Local redox conditions and size of global–regional oxidised SeO_x^{2-} reservoir.	Ferruginous anoxia	shales	
	$\delta^{34}S$	Size of global marine sulfate reservoir and global proportional pyrite burial flux	Euxinia, atmospheric O_2	Carbonates, evaporites	Variable
Atmospheric	$\delta^{53}Cr$	Atmospheric oxygen	>0.1–1% PAL	Shales, ironstones	
	Wildfire record	Atmospheric oxygen	>70% PAL	Charcoal	

92

93

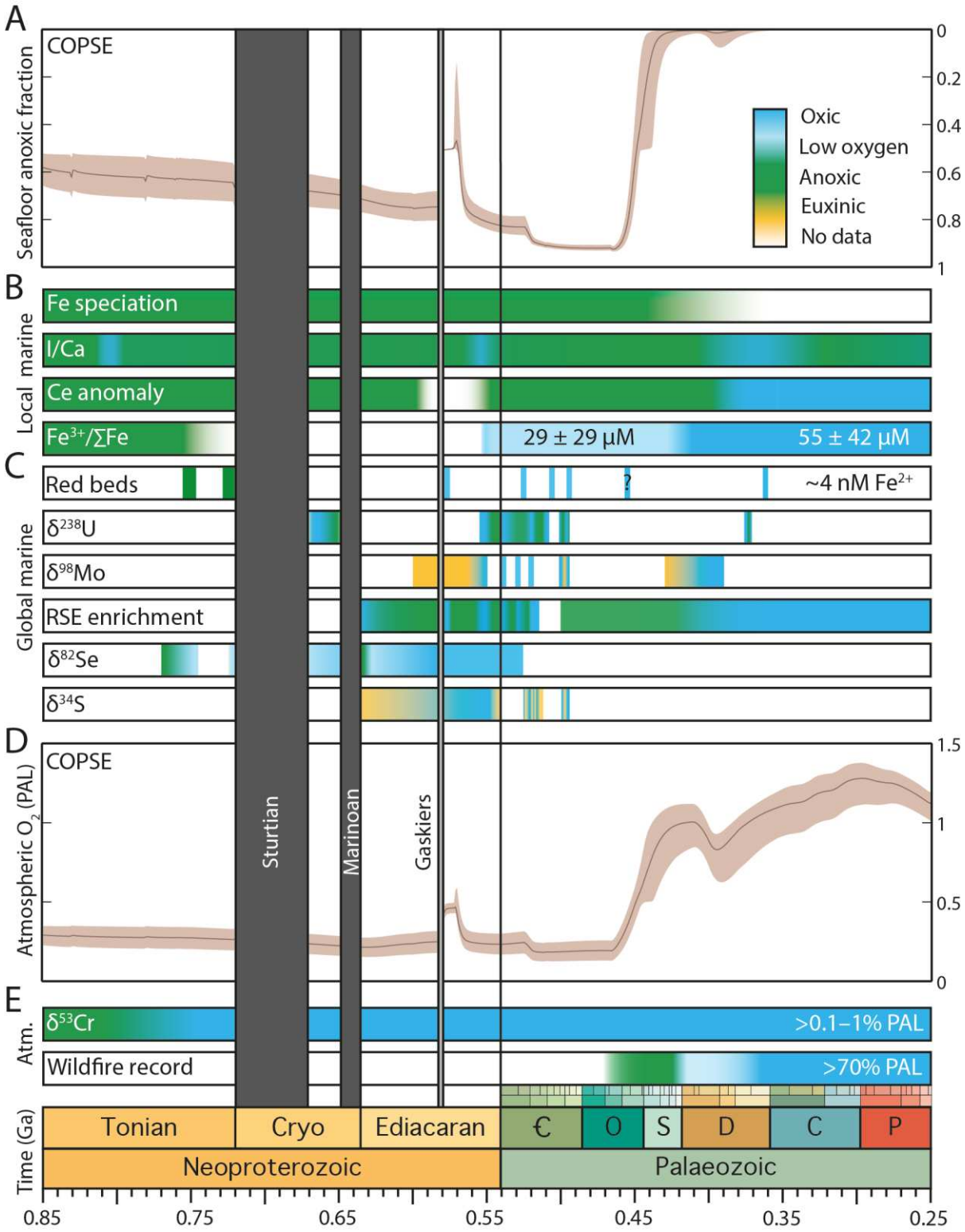

Figure 1. COPSE model predictions of atmospheric and marine redox and inferred redox conditions based on geochemical proxies through the Neoproterozoic and Paleozoic. *A. Modelled seafloor anoxia. Shaded area shows bounds of 10,000 sensitivity analyses. B. Proxy*

inferences for local marine oxygenation, indicating dominantly euxinic (yellow), anoxic (green), low oxygen (light blue), and oxic (dark blue) conditions. Surface waters have contained some oxygen since the GOE, but these interpretations represent the dominant redox conditions. Therefore, a green bar does not imply that the entire ocean was anoxic. For interpretation of each data set, and relevant references, see discussion in the text. C. Proxy inferences for global marine oxygenation. D. Modelled atmospheric O_2 (PAL). E. Proxy inferences for atmospheric O_2.

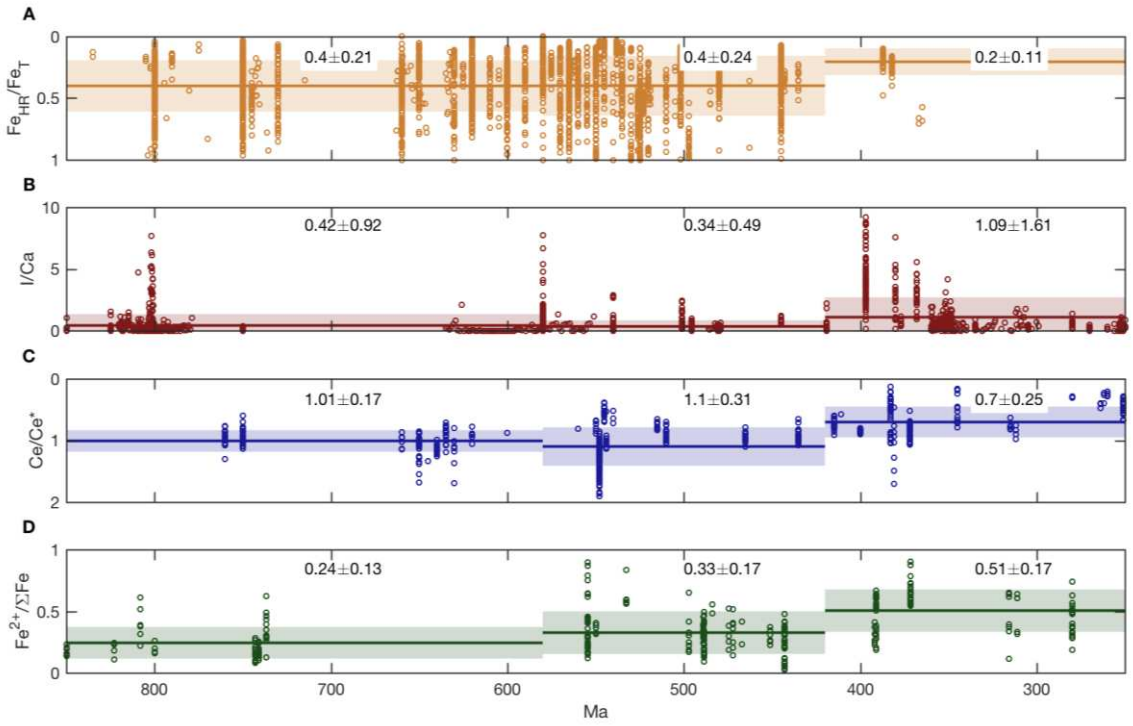

***Figure 2**: **Geochemical data for local–regional redox proxies from 850–250 Ma.** Data (open circles) for Fe speciation from shales[14], I/Ca ratios in carbonate rocks[10,27–29], Ce anomalies in carbonate rocks[30–32] and $Fe^{2+}/\sum Fe$ ratios of seafloor basalts[15]. The average (solid line) and an error window of 1 standard deviation (shaded region) is shown for time bins 850–580, 580–420 and 420–250 Ma.*

I/Ca ratios:

Iodine to calcium ratios in carbonate rocks reflect local water column redox conditions. Since the reduction of iodate (IO_3^-) to iodide (I^-) has a relatively high reduction potential, the I/Ca proxy is sensitive to intermediate redox conditions, from hypoxic (<70–100 μM O_2) to suboxic (manganous – nitrogenous conditions)[33] (Table 1). Iodate is incorporated into carbonate rocks, and so I/Ca ratios reflect the oxidised iodate concentration in the local water column at the depth of carbonate formation, which varies with the concentration of oxygen in surface waters and the depth of the top of the OMZ[10]. Due to the slow kinetics of iodide oxidation, water masses with fluctuating redox conditions, or anoxia nearby, may retain a low iodate signature, biasing primary signatures towards anoxic conditions. In addition, diagenesis can reduce the I/Ca ratio, but not increase it, systematically biasing the rock record towards anoxic conditions[27].

I/Ca data span a large range at any given location, but if there are sufficient data, then an increases in the maximum I/Ca may indicate oxygenation. Long term compilations reveal variable but low I/Ca across the Neoproterozoic and Early Palaeozoic[27] (Figure 2), with notable peaks during the Bitter Springs (~810–800 Ma)[29] and the Shuram excursion (~560 Ma)[27,34]. I/Ca ratios show a significant peak in the Devonian, between ~400 and ~350 Ma, but a return to lower values in the Carboniferous and Permian (Figure 1 and 2)[10]. There is no permanent change towards higher I/Ca ratios until the early Mesozoic. The maximum I/Ca recorded in any given time window may evolve as more data are collected.

Ce anomalies

Negative Ce anomalies in rare earth element patterns are indicative of locally oxic water column conditions. Under oxidising conditions, Ce(III) is oxidised to Ce(IV) on the surface of Mn (oxyhydr)oxide minerals, resulting in relative depletion in shale-normalised seawater Ce concentrations compared with the other rare earth elements. The generation of Ce anomalies requires oxidation of Mn and Ce, both of which have relatively high reduction potentials (+1.23 mV and +1.44 mV, respectively). Therefore, Ce anomalies are responsive to the onset of manganous conditions, which may overlap with low oxygen concentrations (<10 μM). Ce anomalies can respond to redox changes over meter scales[35], although in the open ocean, local signals may be overprinted by basin-wide signals due to slow kinetics[30] (Table 1). The magnitude of any Ce anomaly may correspond to the concentration of oxygen or the thickness of the oxic layer, but can also be influenced by other factors such as local Mn oxide fluxes[36]. Rare earth elements, and associated Ce anomalies, substitute for Ca^{2+} in the carbonate mineral lattice, and as such, can faithfully record seawater REE at the site of carbonate formation, and are relatively robust to diagenesis and even dolomitisation[31,37].

A progressive increase in the magnitude of the Ce anomaly after 551 Ma in carbonate rocks from South China was interpreted to record an increase in oxygen levels in the shallow marine environment during the late Ediacaran Period[22]. However, reducing signals have since been recorded in contemporaneous rocks from the Nama Group, Namibia[32], suggesting oxygenation was not a global phenomenon. Further, long term compilations of Ce anomaly data from eighteen formations show no significant change until the Late Devonian (~383 Ma; Figures 1 and 2)[30]. However, this broad compilation includes large sample gaps. For example, there is only one sample between ~600 Ma and ~550 Ma.

$Fe^{3+}/\sum Fe$ ratio of submarine basalts

As oxygenated water circulates through seafloor basalts, reduced iron is oxidised to Fe^{3+}. Therefore, the $Fe^{3+}/\sum Fe$ ratio of submarine basalts varies with the magnitude of hydrothermal fluxes and with the oxygen content of bottom waters. As such, seafloor basalts, preserved as ophiolites, can provide a direct record of deep water oxygen concentrations (Table 1). Metamorphism acts to reduce Fe^{3+}, and so could systematically bias the $Fe^{3+}/\sum Fe$ ratio towards lower values.

Long term compilations of $Fe^{3+}/\sum Fe$ data show no significant change across the Archean and Proterozoic (Archean = 0.20 ± 0.04; Palaeo–Mesoproterozoic = 0.26 ± 0.02; Neoproterozoic = 0.26 ± 0.05), but a progressive increase across the Early Palaeozoic (0.34 ± 0.08), Late Palaeozoic (0.47 ± 0.10) and Mesozoic–Cenozoic (0.58 ± 0.11) (Figure 2)[15]. This indicates a progressive increase in oxygen content of the deep ocean from 11 ± 17 $\mu molkg^{-1}$ in the Neoproterozoic, to 29 ± 29 $\mu molkg^{-1}$ in the Early Palaeozoic, 55 ± 42 $\mu molkg^{-1}$ in the Late Palaeozoic, and 80 ± 53 $\mu molkg^{-1}$ in the Mesozoic–Cenozoic (Figure 1). Due to the distribution of rare ophiolites in the geological record, there are large gaps where no data are available, as well as large uncertainties in the age of some samples. For example, there are no data between 736 ± 1.7 Ma and 554.5 ± 136.5 Ma. In the Stolper and Keller (2018) study, the Neoproterozoic time bin is dominated by samples >700 Ma, but samples between 555 and 541 are within range of the Early Palaeozoic average (this is reflected in Figure 1).

Red beds:

The distribution of iron rich rocks through the geological record may reflect ocean redox dynamics and Fe^{2+} concentrations[13]. Iron formation requires Fe^{2+} concentrations >50µM,

183 whereas marine red beds, which are thinner and have lower %Fe, only require >4 nM. Major
184 periods of marine red bed deposition occurred in the mid-Ediacaran, Cambrian, and Late
185 Devonian, with a possible event in the late Silurian[13] (blue on Figure 1). These sporadic
186 events indicate lower deep water Fe concentrations following anoxic events, which could be
187 consistent with more oxygenated deep oceans. This record is biased towards preserved
188 shelf sediments, and may evolve if more examples are documented.
189
190 **2.2 Global Marine Geochemical Proxies**
191 *U isotopes:*
192 The uranium isotope ratio of seawater ($\delta^{238}U$) is sensitive to the global proportion of
193 seafloor overlain by anoxic bottom waters. During reduction of soluble U(VI) to insoluble
194 U(IV) under anoxic conditions, sedimentary U(IV) is enriched in ^{238}U, leaving seawater
195 depleted in ^{238}U. Therefore, when the anoxic sink expands, seawater $\delta^{238}U$ decreases, and
196 this signal can be preserved in carbonates. Organic-rich mudrocks also track changes in
197 seawater $\delta^{238}U$, but the signal is offset by a variable local fractionation factor[38] (Table 1).
198 $\delta^{238}U$ data can be used to calculate the proportion of anoxic seafloor, although these
199 estimates rely on several calibration factors that were determined in modern lakes (e.g., the
200 Black Sea[39]). In particular, the calculations are sensitive to the isotope fractionation during U
201 reduction, but more work is needed to explore how this varies under euxinic and anoxic
202 ferruginous conditions. Above ~20% seafloor anoxia, the proxy begins to saturate[40], and
203 large changes in the proportion of seafloor anoxia only translate into small changes in $\delta^{238}U$.
204 These small changes are within the error introduced by diagenesis[41], which can result in
205 positive $\delta^{238}U$ offsets of <0.3‰.
206

Uranium isotope data are available for parts of the Neoproterozoic–Cambrian record (the post-Sturtian interval, and ~560 to ~510 Ma). These data show large oscillations between high, modern-like $\delta^{238}U$, and very low $\delta^{238}U$, suggesting that long term anoxia was punctuated by ocean oxygenation events at ~660, ~560, ~540 and ~520 Ma (Figure 1)[9,18,19,40,42,43]. Some of these oscillations are confirmed by multiple studies in different basins[9,18,19]. Short-term switches towards anoxic conditions are recorded ~497 Ma[44] and 372 Ma[45]. Placing $\delta^{238}U$ into a quantitative model suggests seafloor anoxia oscillated from >30% during periods of quiescence, to <1% during oxygenation events[18].

Mo isotopes:

High $\delta^{98}Mo$ values preserved in shales indicate globally widespread oxic conditions, under which large negative isotope fractionations occur during adsorption of Mo onto Mn oxides, leaving seawater enriched (Table 1). In contrast, under euxinic conditions, Mo is rapidly and quantitatively removed. Since all known sedimentary Mo sinks have a $\delta^{98}Mo$ below contemporaneous seawater, $\delta^{98}Mo$ measurements only provide a minimum constraint on $\delta^{98}Mo_{SW}$. Further, interpretations of sedimentary $\delta^{98}Mo$ rely on independent proxy evidence for local redox conditions. Changes in $\delta^{98}Mo$ could also result from a switch from euxinic to ferruginous anoxia, with no overall increase in oxygenated waters.

Pulses in $\delta^{98}Mo$ are recorded in between ~550 and ~520 Ma, each one reaching progressively higher $\delta^{98}Mo$ maxima[6]. This was interpreted to indicate progressive marine oxygenation across the Cambrian, but the data contain a lot of scatter, and could also be consistent with discrete oxygenation pulses at ~552, ~540, ~530 and ~521 Ma (Figure 1)[6,7,9]. Distinguishing between these two scenarios is difficult because the rarity of black shales

deposited under fully euxinic conditions limits the resolution of the record. The magnitude of δ^{98}Mo enrichments increases through time, suggesting each oxygenation event was more significant than the last[6]. δ^{98}Mo reaches stable, modern-like levels between the mid-Silurian and mid-Devonian (~430–390 Ma)[7]. Modelling calculations suggest that oxygenation events in the Neoproterozoic were limited (33% oxic seafloor)[6,7], but reached >97% oxic seafloor by ~520 Ma, although many of the parameters in these models are poorly constrained.

Redox sensitive elements:

Because Mo is scavenged from seawater under euxinic conditions, and V, U, Re and Cr are scavenged under ferruginous conditions, an increase in the concentration of redox sensitive elements (RSE) in seawater can indicate the global retreat of anoxic sinks. RSE concentrations in shales are controlled by the size of the global RSE reservoir and an enrichment factor, which varies with the local redox conditions. RSE concentrations are commonly analysed in sediments where there is independent evidence for local euxinia, to ensure a consistent local enrichment factor, meaning any enrichments in RSE can be attributed to an expanded global marine RSE reservoir (Table 1). RSE data typically show large amounts of scatter, but an increase in the average or maximum concentration can be interpreted as evidence for an increase in the area of oxic seafloor.

Long term compilations appeared to show an abrupt increase in Mo, V and U concentrations between 663 and 551 Ma[3,46], interpreted to mark widespread oxygenation of the oceans[2]. A recent re-analysis of the U record shows that there is a statistically significant increase in average U concentrations between the Cambrian–Silurian and Devonian–Permian, suggesting any step change towards more permanently oxygenated oceans occurred in the

255 Palaeozoic (Figure 1)[14,46]. The precise timing of any change will depend on the positions of
256 relatively long timescale bins used for data analysis. However, a more complete
257 stratigraphic record with higher sampling density, from a demonstrably open ocean section
258 in Wuhe, South China, has revealed pulses of RSE enrichment at regular intervals,
259 representing ocean oxygenation events at ~635, ~580, ~560, ~540, ~530 and ~522 Ma
260 (Figure 1)[17]. Similar enrichments are observed in other sections located on different cratons,
261 suggesting a truly global signal[7,20,21]. In between these oxygenation events, the widespread
262 anoxia that characterises much of the Proterozoic returns. Modelling efforts suggest that
263 relatively limited seafloor euxinia (1–10%) and more extensive seafloor anoxia (>30–40%)
264 are needed to crash the global Mo and Cr reservoirs, respectively[47].
265
266 *Se isotopes*:
267 Se isotopes (δ^{82}Se) in marine shales are a novel tracer for ocean–atmosphere oxygenation.
268 Se has a reduction potential between S(–II)/S(IV) and Fe(III)/Fe(II), and a relatively short
269 marine residence time (1,100–26,000 years)[48]. During oxyanion (SeO_x^{2-}) reduction under
270 anoxic conditions, isotopically light Se is sequestered into the sediments, driving surface
271 waters isotopically heavy. In addition, an increase in the size of the SeO_x^{2-} reservoir
272 correlates with larger fractionations in locally suboxic sediments (Table 1). Sediments
273 deposited in oxic open oceans, or below well connected OMZs, have lower δ^{82}Se than those
274 from restricted anoxic basins, due to the larger SeO_x^{2-} reservoir. δ^{82}Se yields insight into the
275 local water column redox conditions, with an additional global control. The signal may be
276 further complicated by variations in riverine input, locally enhanced productivity, or basin
277 restriction.
278

279 A progressive decrease in $\delta^{82}Se$ is recorded in shales across the Ediacaran, reaching a
280 minimum around the end of the Ediacaran Period[12]. For the pre-Gaskiers record, the signal
281 is confirmed in multiple sections, suggesting a global control. This is probably a reflection of
282 an increasing SeO_x^{2-} reservoir, which could reflect ocean oxygenation. Overall, the record is
283 difficult to interpret, but suggests a slow but steady shift from fully anoxic to fully oxic deep
284 waters between ~750 and ~540 Ma.
285
286 *S isotopes*:
287 Under euxinic conditions, microbial sulfate reduction converts sulfate (SO_4^{2-}) into sulfide
288 (HS^-), which may be buried as pyrite. The $\delta^{34}S$ of seawater sulfate is sensitive to the global
289 pyrite burial flux, and the isotope fractionation associated with that pyrite burial. Both of
290 these parameters are closely tied to ocean–atmosphere redox (Table 1). The $\delta^{34}S$ signature
291 of seawater is complex[49], but higher $\delta^{34}S_{SO4}$ could indicate enhanced pyrite burial, which
292 may be driven by expanded euxinia. Large offsets between $\delta^{34}S_{SO4}$ and $\delta^{34}S_{pyr}$ ($\Delta^{34}S_{SO4\text{-}pyr}$)
293 have been interpreted to result from a larger marine sulfate reservoir, as well as complex
294 sulfur cycling associated with oxidative side of the S cycle, both of which are associated with
295 higher oxygen levels. At modern marine sulfate concentrations, the $\delta^{34}S$ of seawater should
296 be globally homogeneous, and is preserved in carbonate rocks and evaporites.
297
298 Sedimentary records shows a progressive increase in $\Delta^{34}S_{SO4\text{-}pyr}$ across the Ediacaran (635–
299 ~550 Ma)[8], interpreted to represent an increase in the marine sulfate reservoir, and then
300 the onset of oxidative sulfur cycling. The $\Delta^{34}S_{SO4\text{-}pyr}$ decreases again in the late Ediacaran
301 (~550 Ma), along with an increase in $\delta^{34}S_{SO4}$, suggesting increased pyrite burial and a return
302 to anoxia[50]. However, subsequent work has questioned the link between $\Delta^{34}S_{SO4\text{-}pyr}$ and

oxidative sulfur cycling[51]. A series of rapid oscillations in $\delta^{34}S_{SO4}$ are recorded 524–512 Ma[16], coincident with excursions in with $\delta^{13}C_{carb}$, where the rising limbs are associated with periods of ocean anoxia and increased pyrite burial. This increase in net pyrite burial would produce a pulse of atmospheric oxygen, in turn driving anoxia from the shelf. Further $\delta^{34}S_{SO4}$ oscillation are recorded ~500 Ma[44]. Sulfur isotopes therefore support dynamic redox conditions into the Cambrian and beyond.

2.3 Constraints on atmospheric oxygen

Cr isotopes

The oxidation and reduction of Cr between Cr(III) and Cr(IV) results in large fractionations. Cr oxidation occurs through dissolution of Cr(III) in soils and reaction with Mn oxides, the presence of which is linked to free O_2. This yields dissolved Cr(VI) species (CrO_4^{2-} and $HCrO_4^-$) that are more soluble, and enriched in the heavy isotope, compared with Cr(III). Therefore, under reducing conditions, the marine Cr record in shales and ironstones will be dominated by unfractionated crustal Cr(III), whereas under an oxidising atmosphere, the Cr record will be isotopically enriched.

The long term $\delta^{53}Cr$ record shows a marked enrichment between 800 and 750 Ma[11], recorded in both shales and ironstones, and interpreted to indicate a rise in atmospheric O_2 concentrations. Although the pre-800 record is dominated by low $\delta^{53}Cr$, isolated examples of ^{53}Cr enrichments have been recorded[52]. Cr(III) oxidation during weathering is dependent on Mn oxide availability. Quantitative modelling suggests Mn oxide formation occurs at low O_2 (>0.1–1% PAL), providing a maximum constraint on pre-800 Ma atmosphere[11], and suggesting a modest increase in atmospheric O_2 around 800–750 Ma.

Wildfire record

Wildfires can only be sustained when atmospheric oxygen levels are high (>15–17%)[53]. Charcoal, the geological expression of palaeo-wildfires, is present in the geological record from the latest Silurian onwards[54]. Charcoal is low in abundance across the Silurian and Devonian, but increases by 1–2 orders of magnitude in the late Devonian[55]. This suggests oxygen crossed a critical threshold in the Late Silurian (>15%), but rose further in the Late Devonian (>17%). Wildfires are dependent on the presence of land plants, which evolved ~470 Ma, so the charcoal record cannot constrain pre-Ordovician pO_2.

3. Reconciling proxy records

Direct proxies for atmospheric oxygen are scarce. Chromium isotopic fractionations indicate that O_2 rose above 0.1–1% of present atmospheric levels (PAL) at around 800 Ma[11], however earlier evidence for fractionation of chromium has been recorded[52]. More certain is a rise in O_2 to >70% PAL during the Late Silurian, and a final rise towards modern levels in the Devonian (>80% PAL or above)[55,56]. Regardless of atmospheric oxygen concentrations, substantial spatial and temporal variability is expected in marine redox conditions, as water column O_2 is controlled by a balance between the oxygen supply and its utilization during remineralization. Modelling calculations suggest that widespread deep ocean oxygenation requires atmospheric oxygen to exceed 30–40% PAL, but this depends on the availability of the limiting nutrient phosphate[57], and on the model itself. That said, to first order, deep water oxygenation would be expected to track a substantial rise in atmospheric oxygen levels.

Some global marine geochemical proxies record a permanent change towards widespread oxygenation in the late Palaeozoic, including δ^{98}Mo and U enrichments[7,14,46]. Similarly, compilations of local marine redox proxies don't detect any statistically significant change in oxygen availability across the Neoproterozoic, and instead pinpoint widespread marine oxygenation later, in the Late Palaeozoic–Mesozoic: post-Ordovician for Fe speciation[14], Late Devonian for Ce anomalies[30], Late Palaeozoic for $Fe^{3+}/\sum Fe$ ratios[15], and Early Devonian for I/Ca[10]. There is some variability in the precise timing recorded by each proxy, which may be accounted for by their different sensitivity to the spatial extent or location of anoxia, or to increasing redox state. More importantly, the timing of oxygenation in long term data compilations is highly sensitive to sampling density as well as the boundaries of data bins. For example, $Fe^{3+}/\sum Fe$ ratio data are necessarily sparse as they are derived from rare ophiolites. Therefore, these techniques can only be used to make broad comparisons between, e.g., the Early Palaeozoic and Late Palaeozoic. Four compilations of local proxy data, re-analysed using consistent time bins, all show a significant increase in oxygenation in the period 420–250 Ma compared with 580–420 Ma (Figure 2).

Broadly anoxic Neoproterozoic–Early Palaeozoic oceans could manifest as oxic surface waters overlying fully anoxic deep waters in a 'pancake' structure (Figure 3a), or as shallow, expanded OMZs (Figure 3b and c). A four dimensional transect of local redox conditions across a shelf suggests that OMZ-like structures were established by the Cambrian Period[58], implying that the deep ocean contained low levels of oxygen. This is consistent with $Fe^{3+}/\sum Fe$ ratios[15] and the marine red bed record[13], which support low levels of oxygen in

374 deep waters from the mid-Ediacaran onwards. A shallower OMZ could be a reflection of
375 lower atmospheric oxygen levels, but could also result from differences in carbon cycling.
376
377 If there were indeed mildly oxidising conditions in the deep ocean, then how do we
378 reconcile this with global redox proxies that suggest widespread marine anoxia? Global
379 redox proxies tend to record the percentage of seafloor, globally, that is overlain by anoxic
380 bottom waters, but don't provide insight into the location of those anoxic waters. This is
381 further complicated by the lack of information available on marine productivity, sinking
382 fluxes and ocean circulation, which are key controls on OMZ characteristics. Shallowing of
383 oxygen minimum zones can result in a much larger contact area between anoxic waters and
384 the continental shelf, translating into a larger area of anoxic seafloor, despite no change in
385 the thickness of the OMZ[59] (Figure 3c and 3d). If the OMZ also expanded in thickness, the
386 combined effect could result in the estimated >10–30% seafloor anoxia and >1% seafloor
387 euxinia required to generate anoxic δ^{98}Mo, δ^{238}U and U-enrichment signals (Figure 3b).
388 Furthermore, if bottom waters in the deep ocean were oxic, but contained only low levels of
389 oxygen (<10 µM), then shallow pore waters would be commonly driven anoxic, which may
390 further contribute to anoxic draw down of RSE such as Mo and U.

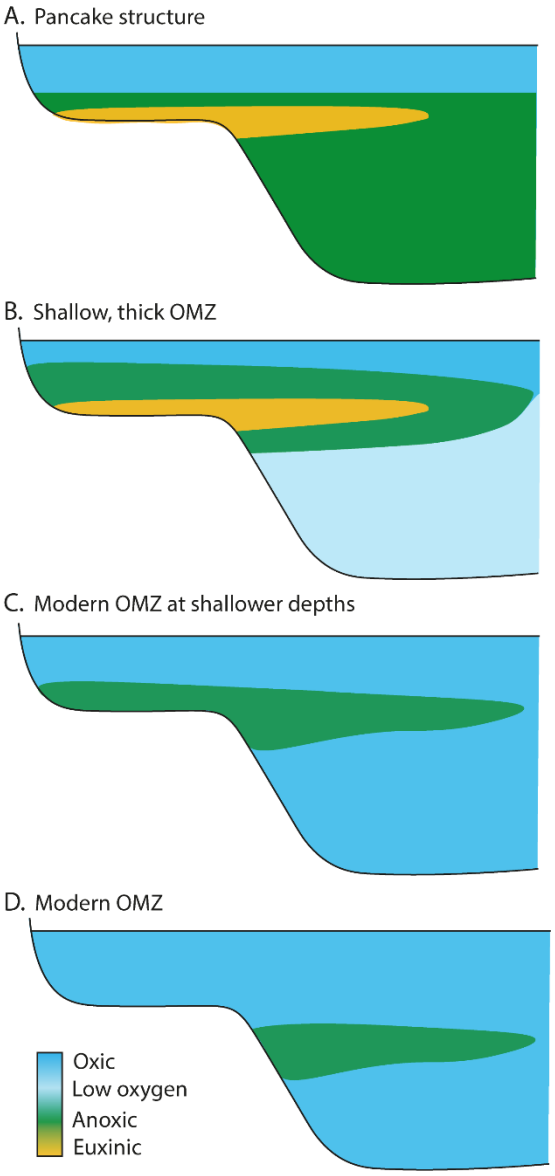

Figure 3. Cartoon showing various possible redox structures for early oceans.

Although large areas of the seafloor remained anoxic or contained only low levels of oxygen through the Neoproterozoic–Lower Palaeozoic, some proxy systems suggest conditions were dynamic, with brief ocean oxygenation events (OOEs). Some OOEs are recorded independently by multiple proxy systems. For example, the transition back towards anoxic conditions following the ~550 Ma OOE is recorded by δ^{98}Mo, δ^{238}U, RSE enrichments, I/Ca ratios and δ^{34}S (Figure 1)[8,9,17,18,27,50]. In contrast, OOEs are not detected in any compilations

of local proxy data. For I/Ca ratio and Ce anomaly data, this is likely because sample coverage is too sparse to detect them. For Fe speciation or $Fe^{3+}/\sum Fe$ ratio data, OOEs would not be detected as data are binned into periods orders of magnitude longer than the duration of OOEs, so OOEs are averaged out or not sampled. Therefore, global redox proxies, analysed in continuous, high resolution sections, detect variability that can be missed by compilations of local redox proxies.

4. Modelling the long-term redox transition

Global biogeochemical models can be used to evaluate the processes which have caused the observed oxygenation pattern. The COPSE model[60] is a non-dimensional system (or 'box model'), which computes the operation of the global C-O-P-S cycles over geological timescales, and is based on the pioneering GEOCARB models[61,62]. Like GEOCARB, the key considerations for COPSE are the global weathering, burial and degassing processes that control the transfer of key species between the hydrosphere and the crust. The long-term O_2 sources are burial of either organic carbon or pyrite sulfur in sediments (removal of a reductant leads to net oxygenation), and the O_2 sinks are the uplift and weathering, or subduction and degassing, of these reduced species which consumes O_2. Importantly, COPSE differs from the GEOCARB models in that it is a 'forwards' model, meaning that it computes all processes via an internally-consistent set of biogeochemical rules[63,64], rather than seeking to infer them directly from the geological record. This means that COPSE can produce estimates of key geochemical proxies such as carbonate $\delta^{13}C$, sulfate $\delta^{34}S$ and strontium $^{87}Sr/^{86}Sr$, which are then used to test the 'skill' of the model by comparing to geological data.

The model is subject to 'external forcings': the rate of tectonic CO_2 input, continental uplift and paleogeography, exposed lithological classes, and a variety of switches that represent the evolution of different modes of life which affect global biogeochemistry. Recent reviews are available that describe the latest version of the model[65,66]. Originally COPSE was built for reconstructing the Phanerozoic Earth system, but in the last decade there have been may extensions to apply the model to the late Precambrian. These extensions have tended to focus on single events such as snowball Earth termination[67] or the (~580 Ma) Shuram negative carbon isotope excursion[68]. We now bring together the key modifications of the model to produce a complete suite of simulations over the Neoproterozoic and Paleozoic (see supplementary material for full explanation of model parameters and differential equations).

We begin from the model of Mills et al.[66], which extended the latest major model release[65] by updating the rates of CO_2 degassing and tectonic uplift with new estimates, as well as revising the link between global climate and chemical weathering rates, informed by Phanerozoic temperature and CO_2 proxies. We then add a function for the evolution of bioturbation during the early Cambrian[69]; a function that represents input of reduced species from the mantle[70]; a deep ocean reservoir of dissolved organic carbon[68] and an uplift-weathering event of evaporite sulfate coincident with the Shuram negative carbon isotope anomaly[68]. Each of these additions has been made to the model previously in isolation and the reader is referred to the cited work for more details. To summarize: bioturbating animals are assumed to evolve by 520 Ma and are presumed to increase the re-oxidation of sedimentary organic matter, and drawdown of the nutrient phosphorus; reductant input is assumed to scale with the ridge generation rate and consumes O_2; a deep

448 ocean reservoir of dissolved organic carbon (DOC) is assumed to have built up over the
449 Precambrian and is rapidly oxidised when the deep ocean becomes oxic – driving a sharp
450 negative carbon isotope excursion; and a large sulfate input event occurs at 580 Ma due to
451 the uplift and weathering of Tonian-age evaporite giants. Debate continues about whether
452 an enlarged marine DOC reservoir is required in order to explain Neoproterozoic C isotope
453 dynamics[71], and around the timing of the effects of bioturbation[72]. It is hoped that further
454 analytical and modelling efforts will help to fully resolve these questions. Incorporating
455 these mechanisms into a single consistent model is a part of this process.
456
457 Figure 1 shows the combined COPSE model predictions for atmospheric O_2 and seafloor
458 anoxia over the Neoproterozoic and Paleozoic, and compares them to the proxies discussed
459 earlier. The brown shaded area represents the boundaries of a suite of 10,000 model
460 sensitivity analyses in which the major external forcings (uplift, degassing, lithology) are
461 varied by ±20%. There is some agreement with the proxies for atmospheric O_2: COPSE
462 predicts (far) above 0.1% PAL for the entire Neoproterozoic, a rise to >70% PAL by the
463 Silurian, and to 100% PAL in the Devonian. This broad pattern is controlled by the evolution
464 of land plants, which are assumed to increase the weathering delivery of the nutrient
465 phosphate (which drives marine productivity), and also the burial of terrestrially-derived
466 organic carbon[55]. Other key features of the atmospheric O_2 predictions are a spike between
467 580–570 Ma, caused by uplift and weathering of evaporite sulfate which stimulates pyrite
468 burial[68], and a drop during the Cambrian coincident with the evolution of significant
469 bioturbation, which limits organic carbon preservation[69]. The only area of substantial
470 disagreement with proxies is that COPSE does not produce lower atmospheric O_2 before
471 ~800 Ma, whereas the lack of fractionation in the Chromium isotope record suggests O_2

might be below 1% PAL[11]. It is not currently clear how strong the constraint from the Cr isotope record is, given that fractionations have been found in several pre-800 Ma samples[52], but it is also possible that a major process is still missing from COPSE, which if included, would result in lower atmospheric O_2. There are several candidates here, including the lack of explicit productivity-remineralization dynamics in the ocean, or a better representation of Precambrian tectonics. Research is ongoing.

The seafloor anoxia prediction from COPSE follows the transitions in atmospheric O_2, with more than 50% of the seafloor anoxic during the Neoproterozoic, and full ventilation during the Devonian. In general agreement with the proxies, there is a period of expanded oxic seafloor immediately post-Gaskiers, which then returns to almost entirely anoxic by the later Cambrian. But there are three major discrepancies between the model predictions and the proxies for seafloor anoxia. Firstly, the model does not produce any of the rapid variability attested to by the proxies (OOEs). Secondly, the model fails to reproduce longer term oxygenation surrounding the Sturtian and Marinoan glaciations. Finally, the model predicts very large anoxic seafloor areas during the later Cambrian and Ordovician, which are not directly supported by any proxies.

The inability of the COPSE model to reproduce the OOEs in the later Ediacaran and Cambrian is probably due to the model's use of a single-box ocean. In COPSE, the shelf environments and (much more vast) deeper ocean are considered to be a single system. This adds a huge amount of buffering capacity, which may not be realistic. A more sophisticated biogeochemical model[73,74] splits the ocean into multiple boxes representing areas of the shelf, open ocean and deep ocean. This model shows that OOEs can occur due

to feedbacks between the marginal phosphorus and oxygen cycles, and thus the lack of OOEs in COPSE may be a consequence of limited representation of shelf environments.

The lack of any appreciable oxygen changes around the Sturtian and Marinoan glaciations is also relatively easily explained, as this version of the COPSE model still does not incorporate any of the processes associated with either the initiation or termination of these snowball Earth events. Looking to the model outputs for sedimentary isotope ratios (Figure 4), it is clear that while the Post-Gaskiers predictions are within reason, the model is missing major aspects of Earth system function pre-600 Ma, especially in the carbon cycle. Here, the large and sustained positive carbon isotope excursions that occur before the Sturtian, and during the aftermath of both glaciations, may represent increased productivity and oxygen production, which is supported by the O_2 proxies.

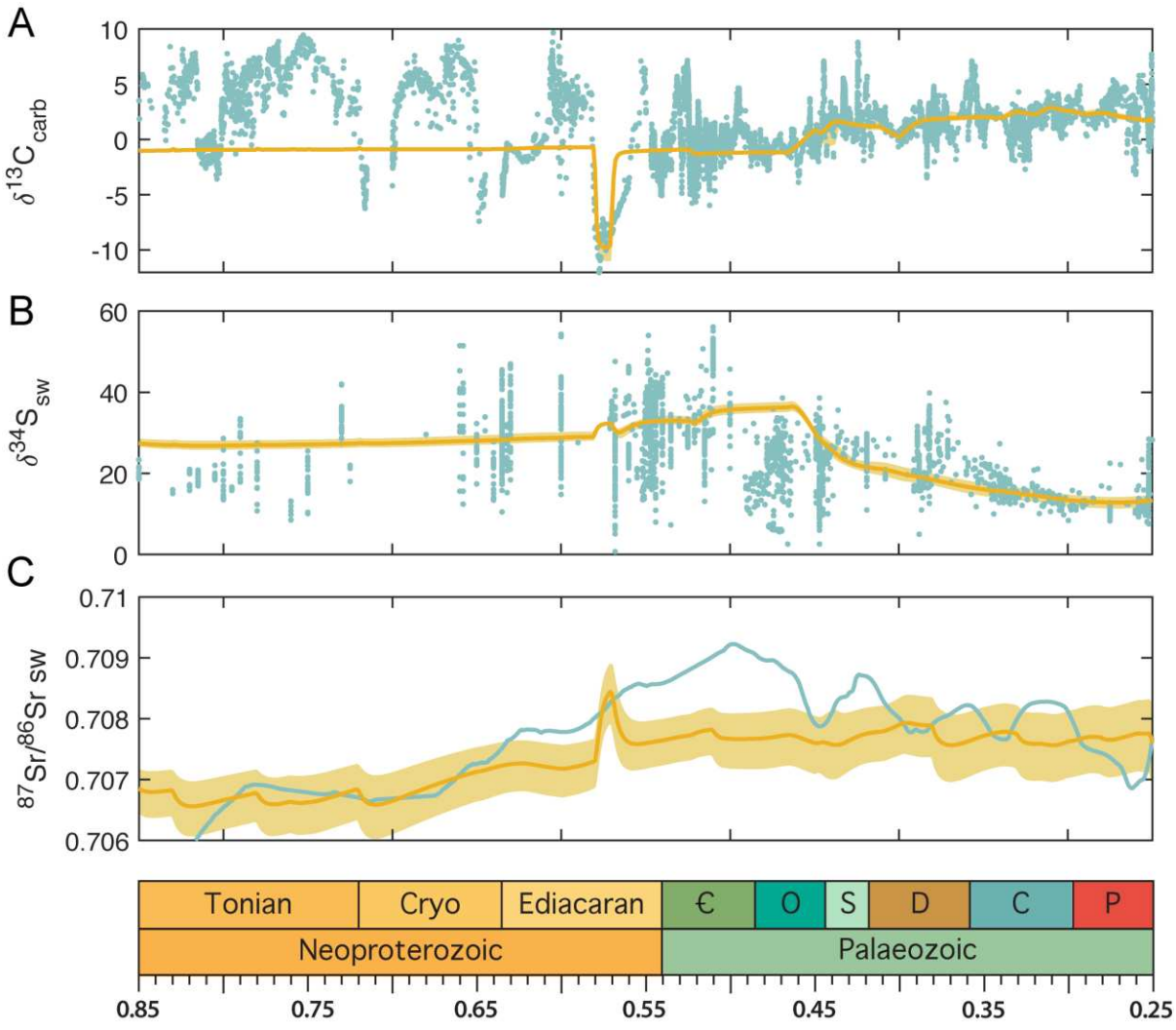

Figure 4. COPSE model isotopic outputs. *Geochemical constraints are shown in teal, and model outputs in yellow. A. $\delta^{13}C$ carbonate sediments. B. $\delta^{34}S$ seawater sulfate. C. $^{87}Sr/^{86}Sr$ carbonate sediments.*

An argument could be made that the break-up of the Rodinia supercontinent was underway by ~750 Ma[75] and led to enhanced continental weathering[76], high rates of organic carbon burial, and high $\delta^{13}C$, before driving the system towards the Sturtian snowball Earth. It is then possible that CO_2 rose to extremely high levels during the glaciations, meaning that the super-greenhouse period that followed glaciation lasted several 10s of Myrs before CO_2 could be reduced to background levels[67]. Adding these ideas into the COPSE model is

possible, but in order to reproduce the timing of isotope excursions, the weathering response to temperature and the effect of erosion on weathering must be very carefully chosen. Thus, we defer further investigation of the dynamics and timing of global glaciations and weathering events in the Cryogenian to spatial models with a better approximation of continental weathering (e.g., GEOCLIM[77,78]).

The large areas of anoxic seafloor during the Cambrian–Ordovician coincide with carbonate $\delta^{13}C$ predictions that sit generally below the data, indicating that the model may be underestimating oxygen production (or incorrectly simulating organic C weathering[79]). This may be due to an over-estimate of the importance of bioturbation in re-oxidising sedimentary organic carbon and burying phosphate. New reaction-transport models of the bioturbation process will hopefully help test this.

5. Assessing the role of oxygen in early animal evolution

The hypothesised rise in oxygen levels across the Neoproterozoic–Palaeozoic has been repeatedly linked to the origin and radiation of early animals[5–7,11,16,80]. Given that oxygen is required by all extant animals, this hypothesis seems intuitive and has proved rather attractive. But a large body of recent work has shown that the role of oxygen in early animal ecosystems is more complex than previously thought[18,81,82]. One issue is that not all geochemical data provide the information needed to address ecologically relevant questions, such as the precise oxygen levels. Waters containing 100 µM or 1 µM O_2 would be indistinguishable in many proxy systems, but the first could host a complex ecosystem containing skeletal animals and motile predators, and the second would be largely uninhabitable[83,84]. These issues can be partly resolved by considering the systematics of

544 each geochemical proxy, and exactly what information they provide about the redox
545 structure of ancient environments.
546
547 Minimum oxygen levels are necessary, but not sufficient, to explain the appearance of new
548 species or ecological traits. Simple sponge-grade animals have very low oxygen demands (1–
549 10 μM)[81], and these requirements appear to have been met continuously in surface waters
550 from at least 800 Ma onwards[11]. During the Neoproterozoic, there may have been
551 progressive increase in the maximum dissolved O_2; enabling the development of more
552 aerobically demanding traits, such as motility and bioturbation. However, for most of the
553 Ediacaran, many proxies suggest widespread anoxic deep waters[18,19]. Ecosystem dynamics,
554 animal distributions, and migration patterns will be influenced by this reduction in habitable
555 space, but clearly, early animal communities continued to thrive in shallow, well-oxygenated
556 shelf environments where their oxygen demands were met[25,32]. It is therefore important to
557 constrain the maximum $O_2(aq)$ available in shelf environments, as well as the spatial extent
558 of inhospitable environments.
559
560 The marine redox landscape in the Cryogenian and Ediacaran appears to have been highly
561 dynamic. It has been suggested that OOEs could have stimulated evolution, and their
562 frequency appears to increase in the late Ediacaran and Cambrian, coincident with an
563 intense period of diversification[17]. Periods of anoxia in between OOEs could even stimulate
564 the development of genetic diversity[82]. Geochemical data and model results suggest that
565 although the Neoproterozoic redox landscape was dynamic, there was no permanent
566 change towards stable, well-oxygenated oceans until at least the Devonian, likely assisted
567 by the evolution of land plants[7,10,14,15,30,55].

6. Conclusions and future directions

The proxy data are best reconciled in the following way: Atmospheric O_2 reached a concentration of >0.1% PAL by around ~800 Ma, and potentially earlier. Surface waters in contact with this atmosphere contained low levels of dissolved oxygen, but the deep oceans remained anoxic. Atmospheric oxygen probably rose in steps or pulses throughout the Cryogenian and Ediacaran, associated with major events such as the break-up of Rodinia, and the Sturtian, Marinoan and Gaskiers glaciations. The post-Sturtian is also marked by the first brief OOEs, which continue into the Cambrian. There is some evidence for OOE magnitude increasing over time[6], and a gradual rise in oxygen over the Neoproterozoic is also consistent with selenium isotope data[12]. By the start of the Cambrian, pO_2 surpassed 30–40% PAL, but oxygen concentrations in much of the deep ocean remained low and the OMZ was thick and shallow. Atmospheric oxygen rose again in the Late Silurian, surpassing 70% PAL, and rose to modern-like levels in the Devonian, pushing the OMZ back off the shelf and establishing modern, well-oxygenated oceans (Figure 3d). The COPSE model is unable to reproduce the full complexity revealed by geochemical data, but does capture first order patterns of atmospheric and marine oxygenation from the Ediacaran onwards, giving confidence that the behaviour we see in the proxies is reasonable. The hypothesised Neoproterozoic Oxygenation Event (NOE) would be more accurately described as a Neoproterozoic Oxygenation Window (NOW), featuring dynamic pulses of oxygenation against a background of gradually rising oxygen levels, and any step change towards stable, well-oxygenated conditions appears to have been delayed until the Palaeozoic Oxygenation Event (POE).

Moving forward, we need to consider which geochemical data can best capture this transition. To understand the timing, frequency and duration of OOEs, we need to target high resolution continuous successions and analyse multiple global redox proxies. To meaningfully address questions surrounding the role of oxygen in early animal ecosystems, we need to focus on developing quantitative constraints on maximum $O_2(aq)$. These could include proxies for atmospheric oxygen, such as Cr isotopes, or marine redox proxies that respond to intermediate redox conditions, such as Ce anomalies and I/Ca. Detailed 4D maps across shelf ecosystems can reveal the structure of marine anoxia (i.e., pancake vs. OMZ), and be tied directly to the fossil record.

Data accessibility

The geochemical data are all published elsewhere, and discussed in full in the relevant references. Differential equations and fixed parameters from the model are available in the supplementary material. All modelling code and outputs can be obtained from BJWM on request.

Author's contributions

R.T. compiled proxy data, and B.J.W.M. modified the COPSE biogeochemical model. R.T. and B.J.W.M discussed the results and wrote the manuscript together.

Competing interests

The authors declare no competing interests

Acknowledgements

We are grateful to Zunli Lu and Noah Planavsky for reviews that helped to improve this manuscript. We thank the Royal Society for supporting us to attend a meeting in London where these ideas were discussed. R.T. is supported by a grant from the DSI-NRF Centre of Excellence in Palaeosciences and B.J.W.M is funded by the UK Natural Environment Research Council (NE/R010129/1 and NE/S009663/1) and by a University of Leeds Academic Fellowship.

References

1. Farquhar, J., Bao, H. & Thiemens, M. Atmospheric Influence of Earth's Earliest Sulfur Cycle. *Science* **289**, 756–758 (2000).
2. Och, L. M. & Shields-Zhou, G. A. The Neoproterozoic oxygenation event: environmental perturbations and biogeochemical cycling. *Earth-Sci. Rev.* **110**, 26–57 (2012).
3. Scott, C. *et al.* Tracing the stepwise oxygenation of the Proterozoic ocean. *Nature* **452**, 456–459 (2008).
4. Canfield, D. E. & Farquhar, J. Animal evolution, bioturbation, and the sulfate concentration of the oceans. *Proc. Natl. Acad. Sci. U. S. A.* **106**, 8123–8127 (2009).
5. Canfield, D. E., Poulton, S. W. & Narbonne, G. M. Late-Neoproterozoic Deep-Ocean Oxygenation and the Rise of Animal Life. *Science* **315**, 92–95 (2007).
6. Chen, X. *et al.* Rise to modern levels of ocean oxygenation coincided with the Cambrian radiation of animals. *Nat. Commun.* **6**, (2015).
7. Dahl, T. W. *et al.* Devonian rise in atmospheric oxygen correlated to the radiations of terrestrial plants and large predatory fish. *Proc. Natl. Acad. Sci.* **107**, 17911–17915 (2010).

8. Fike, D. A., Grotzinger, J. P., Pratt, L. M. & Summons, R. E. Oxidation of the Ediacaran Ocean. *Nature* **444**, 744–747 (2006).
9. Kendall, B. *et al.* Uranium and molybdenum isotope evidence for an episode of widespread ocean oxygenation during the late Ediacaran Period. *Geochim. Cosmochim. Acta* **156**, 173–193 (2015).
10. Lu, W. *et al.* Late inception of a resiliently oxygenated upper ocean. *Science* **361**, 174–177 (2018).
11. Planavsky, N. J. *et al.* Low Mid-Proterozoic atmospheric oxygen levels and the delayed rise of animals. *Science* **346**, 635–638 (2014).
12. Pogge von Strandmann, P. A. E. *et al.* Selenium isotope evidence for progressive oxidation of the Neoproterozoic biosphere. *Nat. Commun.* **6**, 10157 (2015).
13. Song, H. *et al.* The onset of widespread marine red beds and the evolution of ferruginous oceans. *Nat. Commun.* **8**, 1–7 (2017).
14. Sperling, E. A. *et al.* Statistical analysis of iron geochemical data suggests limited late Proterozoic oxygenation. *Nature* **523**, 451–454 (2015).
15. Stolper, D. A. & Keller, C. B. A record of deep-ocean dissolved O_2 from the oxidation state of iron in submarine basalts. *Nature* **553**, 323 (2018).
16. He, T. *et al.* Possible links between extreme oxygen perturbations and the Cambrian radiation of animals. *Nat. Geosci.* **12**, 468–474 (2019).
17. Sahoo, S. K. *et al.* Oceanic oxygenation events in the anoxic Ediacaran ocean. *Geobiology* **14**, 457–468 (2016).
18. Tostevin, R. *et al.* Uranium isotope evidence for an expansion of anoxia in terminal Ediacaran oceans. *Earth Planet. Sci. Lett.* **506**, 104–112 (2019).

19. Zhang, F. *et al.* Extensive marine anoxia during the terminal Ediacaran Period. *Sci. Adv.* **4**, eaan8983 (2018).
20. Kurzweil, F. *et al.* Coupled sulfur, iron and molybdenum isotope data from black shales of the Teplá-Barrandian unit argue against deep ocean oxygenation during the Ediacaran. *Geochim. Cosmochim. Acta* **171**, 121–142 (2015).
21. Johnston, D. T. *et al.* Searching for an oxygenation event in the fossiliferous Ediacaran of northwestern Canada. *Chem. Geol.* **362**, 273–286 (2013).
22. Ling, H.-F. *et al.* Cerium anomaly variations in Ediacaran–earliest Cambrian carbonates from the Yangtze Gorges area, South China: implications for oxygenation of coeval shallow seawater. *Precambrian Res.* **225**, 110–127 (2013).
23. Poulton, S. W. & Canfield, D. E. Development of a sequential extraction procedure for iron: implications for iron partitioning in continentally derived particulates. *Chem. Geol.* **214**, 209–221 (2005).
24. Canfield, D. E. *et al.* Ferruginous Conditions Dominated Later Neoproterozoic Deep-Water Chemistry. *Science* **321**, 949–952 (2008).
25. Wood, R. A. *et al.* Dynamic redox conditions control late Ediacaran ecosystems in the Nama Group, Namibia. *Precambrian Res.* **261**, 252–271 (2015).
26. Boyer, D. L., Owens, J. D., Lyons, T. W. & Droser, M. L. Joining forces: Combined biological and geochemical proxies reveal a complex but refined high-resolution palaeo-oxygen history in Devonian epeiric seas. *Palaeogeogr. Palaeoclimatol. Palaeoecol.* **306**, 134–146 (2011).
27. Hardisty, D. S. *et al.* Perspectives on Proterozoic surface ocean redox from iodine contents in ancient and recent carbonate. *Earth Planet. Sci. Lett.* **463**, 159–170 (2017).

685 28. Uahengo, C.-I., Shi, X., Jiang, G. & Vatuva, A. Transient shallow-ocean oxidation
686 associated with the late Ediacaran Nama skeletal fauna: Evidence from iodine contents
687 of the Lower Nama Group, southern Namibia. *Precambrian Res.* 105732 (2020)
688 doi:10.1016/j.precamres.2020.105732.
689 29. Lu, W. *et al.* Iodine proxy evidence for increased ocean oxygenation during the Bitter
690 Springs Anomaly. *Geochem. Perspect. Lett.* **5**, 53–57 (2017).
691 30. Wallace, M. W. *et al.* Oxygenation history of the Neoproterozoic to early Phanerozoic
692 and the rise of land plants. *Earth Planet. Sci. Lett.* **466**, 12–19 (2017).
693 31. Nothdurft, L. D., Webb, G. E. & Kamber, B. S. Rare earth element geochemistry of Late
694 Devonian reefal carbonates, Canning Basin, Western Australia: confirmation of a
695 seawater REE proxy in ancient limestones. *Geochim. Cosmochim. Acta* **68**, 263–283
696 (2004).
697 32. Tostevin, R. *et al.* Low-oxygen waters limited habitable space for early animals. *Nat.*
698 *Commun.* **7**, (2016).
699 33. Lu, W. *et al.* Refining the planktic foraminiferal I/Ca proxy: Results from the Southeast
700 Atlantic Ocean. *Geochim. Cosmochim. Acta* (2019) doi:10.1016/j.gca.2019.10.025.
701 34. Macdonald, F. A. *et al.* The stratigraphic relationship between the Shuram carbon
702 isotope excursion, the oxygenation of Neoproterozoic oceans, and the first appearance
703 of the Ediacara biota and bilaterian trace fossils in northwestern Canada. *Chem. Geol.*
704 **362**, 250–272 (2013).
705 35. De Carlo, E. H. & Green, W. J. Rare earth elements in the water column of Lake Vanda,
706 McMurdo Dry Valleys, Antarctica. *Geochim. Cosmochim. Acta* **66**, 1323–1333 (2002).

36. O'Connell, B., Wallace, M. W., Hood, A. v. S., Lechte, M. A. & Planavsky, N. J. Iron-rich carbonate tidal deposits, Angepena Formation, South Australia: A redox-stratified Cryogenian basin. *Precambrian Res.* **342**, 105668 (2020).
37. Banner, J. L., Hanson, G. N. & Meyers, W. J. Rare Earth Element and Nd Isotopic Variations in Regionally Extensive Dolomites From the Burlington-Keokuk Formation (Mississippian): Implications for Ree Mobility During Carbonate Diagenesis. *J. Sediment. Res.* **58**, (1988).
38. Lau, K. V., Romaniello, S. J. & Zhang, F. The Uranium Isotope Paleoredox Proxy. *Elements in Geochemical Tracers in Earth System Science* /core/elements/uranium-isotope-paleoredox-proxy/200458FA5D3F890D690C8907FEF738D7 (2019) doi:10.1017/9781108584142.
39. Rolison, J. M., Stirling, C. H., Middag, R. & Rijkenberg, M. J. A. Uranium stable isotope fractionation in the Black Sea: Modern calibration of the 238U/235U paleo-redox proxy. *Geochim. Cosmochim. Acta* **203**, 69–88 (2017).
40. Lau, K. V., Macdonald, F. A., Maher, K. & Payne, J. L. Uranium isotope evidence for temporary ocean oxygenation in the aftermath of the Sturtian Snowball Earth. *Earth Planet. Sci. Lett.* **458**, 282–292 (2017).
41. Chen, X. *et al.* Diagenetic effects on uranium isotope fractionation in carbonate sediments from the Bahamas. *Geochim. Cosmochim. Acta* **237**, 294–311 (2018).
42. Dahl, T. W. Reorganisation of Earth's biogeochemical cycles briefly oxygenated the oceans 520 Myr ago. *Geochem. Perspect. Lett.* **3**, 210–220 (2017).
43. Wei, G.-Y. *et al.* Marine redox fluctuation as a potential trigger for the Cambrian explosion. *Geology* **46**, 587–590 (2018).

730 44. Dahl, T. W. *et al.* Uranium isotopes distinguish two geochemically distinct stages during
731 the later Cambrian SPICE event. *Earth Planet. Sci. Lett.* **401**, 313–326 (2014).
732 45. White, D. A., Elrick, M., Romaniello, S. & Zhang, F. Global seawater redox trends during
733 the Late Devonian mass extinction detected using U isotopes of marine limestones.
734 *Earth Planet. Sci. Lett.* **503**, 68–77 (2018).
735 46. Partin, C. A. *et al.* Large-scale fluctuations in Precambrian atmospheric and oceanic
736 oxygen levels from the record of U in shales. *Earth Planet. Sci. Lett.* **369–370**, 284–293
737 (2013).
738 47. Reinhard, C. T. *et al.* Proterozoic ocean redox and biogeochemical stasis. *Proc. Natl.*
739 *Acad. Sci.* **110**, 5357–5362 (2013).
740 48. Fernández-Martínez, A. & Charlet, L. Selenium environmental cycling and bioavailability:
741 a structural chemist point of view. *Rev. Environ. Sci. Biotechnol.* **8**, 81–110 (2009).
742 49. Fike, D. A., Bradley, A. S. & Rose, C. V. Rethinking the Ancient Sulfur Cycle. *Annu. Rev.*
743 *Earth Planet. Sci.* **43**, 593–622 (2015).
744 50. Ries, J. B., Fike, D. A., Pratt, L. M., Lyons, T. W. & Grotzinger, J. P. Superheavy pyrite
745 (δ34Spyr > δ34SCAS) in the terminal Proterozoic Nama Group, southern Namibia: A
746 consequence of low seawater sulfate at the dawn of animal life. *Geology* **37**, 743–746
747 (2009).
748 51. Sim, M. S., Bosak, T. & Ono, S. Large Sulfur Isotope Fractionation Does Not Require
749 Disproportionation. *Science* **333**, 74–77 (2011).
750 52. Canfield, D. E. *et al.* Highly fractionated chromium isotopes in Mesoproterozoic-aged
751 shales and atmospheric oxygen. *Nat. Commun.* **9**, 1–11 (2018).
752 53. Belcher, C. M. & McElwain, J. C. Limits for Combustion in Low O2 Redefine
753 Paleoatmospheric Predictions for the Mesozoic. *Science* **321**, 1197–1200 (2008).

754 54. Glasspool, I. J., Edwards, D. & Axe, L. Charcoal in the Silurian as evidence for the earliest
755 wildfire. *Geology* **32**, 381–383 (2004).
756 55. Lenton, T. M. *et al.* Earliest land plants created modern levels of atmospheric oxygen.
757 *Proc. Natl. Acad. Sci.* **113**, 9704–9709 (2016).
758 56. Glasspool, I. J. & Scott, A. C. Phanerozoic concentrations of atmospheric oxygen
759 reconstructed from sedimentary charcoal. *Nat. Geosci.* **3**, 627–630 (2010).
760 57. Canfield, D. E. A new model for Proterozoic ocean chemistry. *Nature* **396**, 450–453
761 (1998).
762 58. Guilbaud, R. *et al.* Oxygen minimum zones in the early Cambrian ocean. *Geochem.*
763 *Perspect. Lett.* **6**, 33–38 (2018).
764 59. Lau, K. V. *et al.* Marine anoxia and delayed Earth system recovery after the end-Permian
765 extinction. *Proc. Natl. Acad. Sci.* **113**, 2360–2365 (2016).
766 60. Bergman, N. M., Lenton, T. M. & Watson, A. J. COPSE: a new model of biogeochemical
767 cycling over Phanerozoic time. *Am. J. Sci.* **304**, 397–437 (2004).
768 61. Berner, R. A. (Yale U. GEOCARB II: A revised model of atmospheric CO2 over phanerozoic
769 time. *Am. J. Sci. U. S.* **294:1**, (1994).
770 62. Berner, R. A. (Yale U. A model for atmospheric CO2 over phanerozoic time. *Am. J. Sci. U.*
771 *S.* **291:4**, (1991).
772 63. Cappellen, P. V. & Ingall, E. D. Benthic phosphorus regeneration, net primary
773 production, and ocean anoxia: A model of the coupled marine biogeochemical cycles of
774 carbon and phosphorus. *Paleoceanography* **9**, 677–692 (1994).
775 64. Lenton, T. M. & Watson, A. J. Redfield revisited: 2. What regulates the oxygen content of
776 the atmosphere? *Glob. Biogeochem. Cycles* **14**, 249–268 (2000).

65. Lenton, T. M., Daines, S. J. & Mills, B. J. W. COPSE reloaded: An improved model of biogeochemical cycling over Phanerozoic time. *Earth-Sci. Rev.* **178**, 1–28 (2018).
66. Mills, B. J. W. *et al.* Modelling the long-term carbon cycle, atmospheric CO2, and Earth surface temperature from late Neoproterozoic to present day. *Gondwana Res.* **67**, 172–186 (2019).
67. Mills, B., Watson, A. J., Goldblatt, C., Boyle, R. & Lenton, T. M. Timing of Neoproterozoic glaciations linked to transport-limited global weathering. *Nat. Geosci.* **4**, 861–864 (2011).
68. Shields, G. A. *et al.* Unique Neoproterozoic carbon isotope excursions sustained by coupled evaporite dissolution and pyrite burial. *Nat. Geosci.* **12**, 823–827 (2019).
69. van de Velde, S., Mills, B. J. W., Meysman, F. J. R., Lenton, T. M. & Poulton, S. W. Early Palaeozoic ocean anoxia and global warming driven by the evolution of shallow burrowing. *Nat. Commun.* **9**, 1–10 (2018).
70. Williams, J. J., Mills, B. J. W. & Lenton, T. M. A tectonically driven Ediacaran oxygenation event. *Nat. Commun.* **10**, 1–10 (2019).
71. Husson, J. M. *et al.* Large isotopic variability at the micron-scale in 'Shuram' excursion carbonates from South Australia. *Earth Planet. Sci. Lett.* **538**, 116211 (2020).
72. Tarhan, L. G. The early Paleozoic development of bioturbation—Evolutionary and geobiological consequences. *Earth-Sci. Rev.* **178**, 177–207 (2018).
73. Alcott, L. J., Mills, B. J. W. & Poulton, S. W. Stepwise Earth oxygenation is an inherent property of global biogeochemical cycling. *Science* (2019).
74. Slomp, C. P. & Van Cappellen, P. The global marine phosphorus cycle: sensitivity to oceanic circulation. *Biogeosciences Discuss.* **3**, 1587–1629 (2006).

75. Li, Z. X. *et al.* Assembly, configuration, and break-up history of Rodinia: A synthesis. *Precambrian Res.* **160**, 179–210 (2008).
76. Donnadieu, Y., Goddéris, Y., Ramstein, G., Nédélec, A. & Meert, J. A 'snowball Earth' climate triggered by continental break-up through changes in runoff. *Nature* **428**, 303–306 (2004).
77. Goddéris, Y. *et al.* Onset and ending of the late Palaeozoic ice age triggered by tectonically paced rock weathering. *Nat. Geosci.* **10**, 382–386 (2017).
78. Goddéris, Y., Donnadieu, Y., Le Hir, G., Lefebvre, V. & Nardin, E. The role of palaeogeography in the Phanerozoic history of atmospheric CO2 and climate. *Earth-Sci. Rev.* **128**, 122–138 (2014).
79. Daines, S. J., Mills, B. J. W. & Lenton, T. M. Atmospheric oxygen regulation at low Proterozoic levels by incomplete oxidative weathering of sedimentary organic carbon. *Nat. Commun.* **8**, 1–11 (2017).
80. Nursall, J. Oxygen as a prerequisite to the origin of the Metazoa. *Nature* **183**, 1170–1172 (1959).
81. Mills, D. B. *et al.* Oxygen requirements of the earliest animals. *Proc. Natl. Acad. Sci.* **111**, 4168–4172 (2014).
82. Wood, R. & Erwin, D. H. Innovation not recovery: dynamic redox promotes metazoan radiations. *Biol. Rev.* (2017) doi:10.1111/brv.12375.
83. Levin, L. A., Gage, J. D., Martin, C. & Lamont, P. A. Macrobenthic community structure within and beneath the oxygen minimum zone, NW Arabian Sea. *Deep Sea Res.* **47**, 189–226 (2000).
84. Sperling, E. A. *et al.* Oxygen, ecology, and the Cambrian radiation of animals. *Proc. Natl. Acad. Sci.* **110**, 13446–13451 (2013).

824